Supporting Information

Binding forces of cellulose binding modules on cellulosic nanomaterials

Alessandra Griffo[¥], *Bart J. M. Rooijakkers*[¥], *Hendrik Hähl*[‖], *Karin Jacobs*[‖], *Markus B. Linder*[¥], *Päivi Laaksonen*[¥]*

[¥]Department of Bioproducts and Biosystems, Aalto University, Espoo, FI-00076 Aalto, Finland

[‖]Department of Experimental Physics, Saarland University, Saarbrücken 66123 Germany

AFM Images of SpyCatcher-Cel7A-CBM1 on cellulose

AFM images were recorded from the spin-coated cellulose surface after adsorption of the SpyCatcher-Cel7A-CBM1 on the surface. Spehrical grain-like features appeared both in the topography and the phase images.

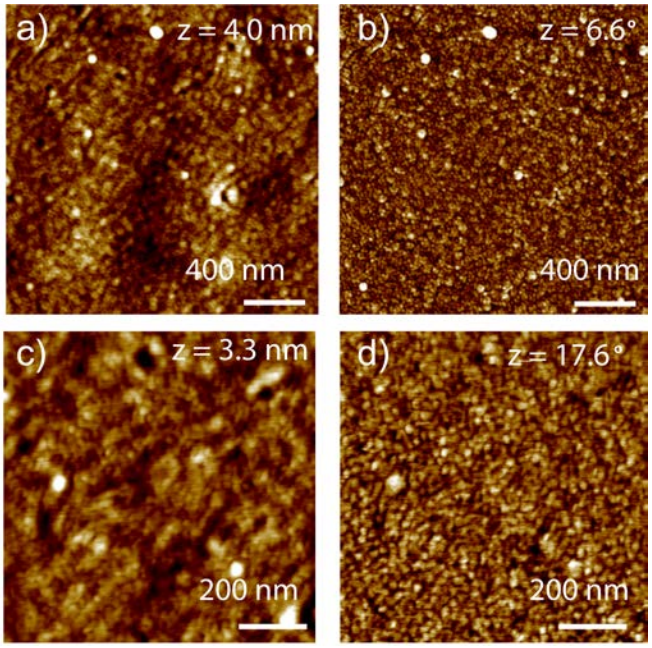

Figure SI 1. AFM height a, c) and phase b, d) images representing a SpyCatcher-CBM1 (Cel7A) fusion protein solution casted on a cellulose spin coated SiO_2 surface. Scan sizes recorded are 2µm b), c) and 1µm d), e). Height range z from black to white is given in each image.

Plasmid design and preparation

In order to obtain a Spycatcher-CBM1 fusion protein, a construct was designed with an N-terminal cleavable Smt3 domain, followed by SpyCatcher, a 22 amino acid flexible linker, the CBM1 domain from Cel7a and a C-terminal His-tag for purification. The Ubiquitin-like SUMO protein from yeast Smt3[1] was chosen as solubility-tag because previous experience indicated good production levels in *E. coli* and since it could be cleaved off with the protease Ulp1. All segments were obtained with PCR (using KAPA HiFi DNA Polymerase from KAPA Biosystems and primers from Eurofins Genomics), all flanked with BsaI restriction sites and appropriate 4bp overlaps. Using the Golden Gate cloning method[2], the pieces were combined and ligated (with BsaI-HF and T4 DNA Ligase from NEB) into a pET28a (+) expression vector and transformed in chemically competent TOP10 *E. coli* cells. The resulting plasmid was

obtained by miniprep (NucleoSpin Plasmid from Macherey-Nagel). The construct was verified by 1% agarose gel electrophoresis and sequencing (Eurofins Genomics).

Figure SI 2. Designed construct with an N-terminal cleavable Smt3 domain, followed by SpyCatcher, a 22 amino acid flexible linker, the CBM1 domain from Cel7a and a C-terminal His-tag for purification.

Single molecule force spectroscopy – adhesion events

Statistics of the observe adhesion events are presented in Table SI 1. The adhesion events are categorized in the following way. 1) Specific adhesion means that there was a clear single rupture peak at a given distance from the surface 2) zero adhesion means that there was no rupture peak at all and 3) non-specific adhesion refers to the retraction curves, where there was a rupture peak at zero distance from the surface. Examples of every event are shown in Figure SI 3.

Table SI 1. Table reporting the *N* experiments with the related concentrations and percentages

	Total Fd curves	Concentration	Specific adhesion	Zero adhesion	Non-specific adhesion
Cellulose (TMSC)	1600	1 µM	6 %	44 %	50 %
CNC(H_2SO_4)	982	1 µM	6.5%	57 %	36.5 %
CNC(HCl)	1436	1 µM	4 %	82 %	14 %
ChNCs	614	10 µM	21 %	57 %	22 %
Cellulose (TMSC)	350	10 µM	~ 80 %	_	~ 20 %

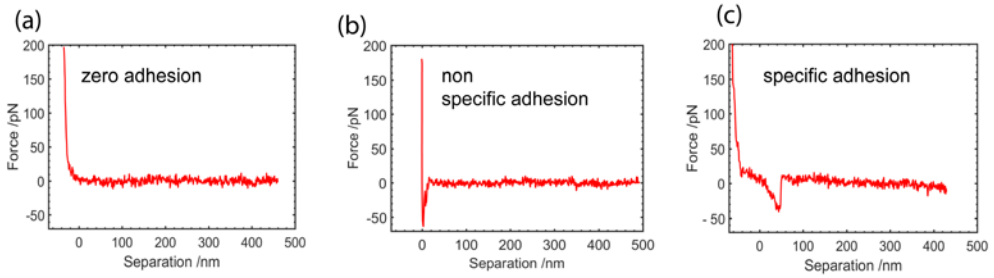

Figure SI 3. Example of three different F_d (CBM1(Cel7A)-cellulose interaction) curves showing respectively zero adhesion a), non-specific adhesion b) and specific adhesion c).

Estimated length of the molecules

The length of the polymer chains were estimated adding up the length of the amino acids and the alkyne-PEG-silane. Length estimates are summarized in Table SI 2.

Table SI 2. Table reporting the theoretically estimated length of the peptides and proteins studied

	Alkyne-PEG-silane*	SpyTag	Linker	SpyCatcher	CBM1	Total
N (aa)	_	15	23	114	48	177
Theoretical length (nm)	17-21*	~ 5.4	8.2	2-4	3	~ 36-42

**Obtained multiplying the length on 1 PEG monomer * n, where n ~49 (n is more an average number taking into account the polydispersity of the polymer)*

FD curves on CNCs discarded from the analysis

Histograms a (CNC_{HCl}) and b ($CNCH_2SO_4$) of Figure SI 4 sum to the data of the FD curves reported in the main text (respectively figure 3 a and b) also the FD curves discarded from the analysis for two reasons: multiple rupture events happens and the fit is not perfectly applicable. However, those curves are also representative of the unbinding force and support our data even though we chose to not report them to simplify the text.

In fact, is interesting to observe that the distribution did not change significantly if compared to the ones reported in the main text: the standard deviation between Figure 3 b and c of the main text and Figure SI 4 respectively a and b is +/- 1.

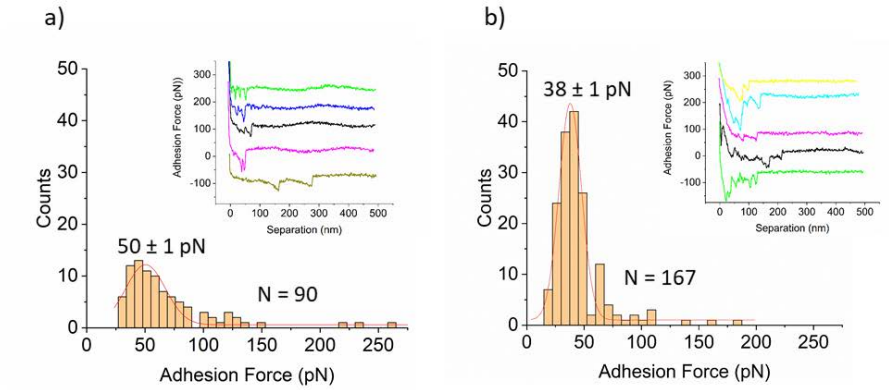

Figure SI 4. Histograms representing the binding force for CNC(HCl) a) and for CNC(H_2SO_4) b).

Single vs. multiple molecule adhesion

Comparison of the retraction curves measured on spin-coated cellulose (from TMSC) and chitin nanocrystals. For these experiments, the AFM tip was functionalized by incubation in 10 µM protein solution. On cellulose, the experiments resulted in adhesion of multiple molecules, whereas on chitin nanocrystals, there was typically only one rupture peak.

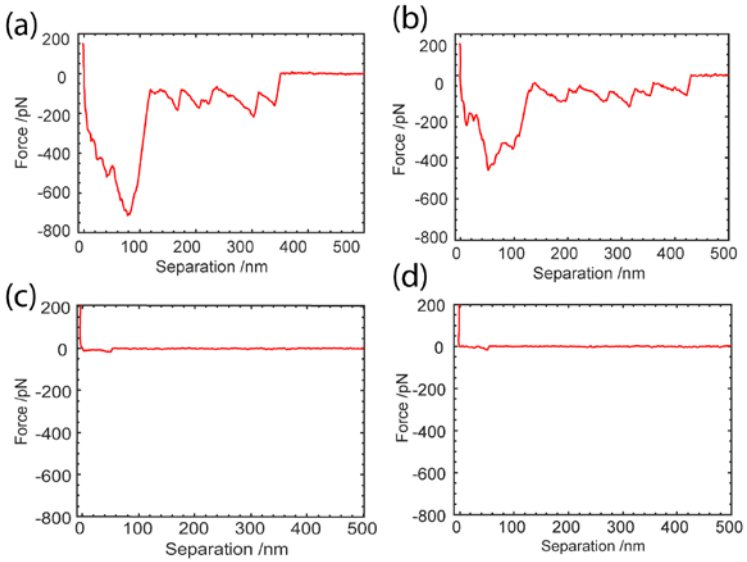

Figure SI 5. Force distance curves related to the CBM1 (Cel7A) –cellulose a,b) and chitin nanocrystals c,d) interaction at a concentration of 10 µM. For CBM1 (Cel7A) – cellulose interaction multiple peaks were observed due to the multiple detachment of the CBM-terminated molecules. In detail, a large peak (< 100 nm) quite likely represented the attachment and detachment of many molecules whereas later (> 150 nm) only individual detachments could be seen For CBM1 (Cel7A) – chitin interaction only individual detachment phenomena were observed.

Optimization of the CNC coatings

Different methods for fixation of the CNCs on the SiO_2 surface were attempted to find the best way of obtaining a stable nanocrystal film with a full surface coverage. AFM images of differenlty prepared surface assemblies are presented in Figure SI 6.

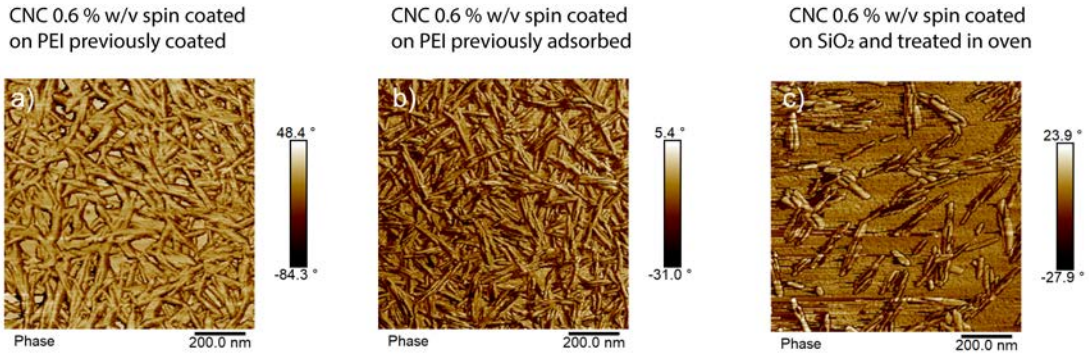

Figure SI 6. AFM phase images of cellulose nanocrystals $CNCs_{(H_2SO_4)}$ spin coated (from left to right) to a PEI previously adsorbed on SiO_2, to a PEI previosly spin coated SiO_2, to a plasma cleaned SiO_2 surface then cured in oven at 80 ˚C for 15 minutes.

Tip functionalization

Each step of the tip functionalization were confirmed by measuring the force-distance curves of the tip on cellulose surface. Typical force curves and their disrtributions are presented in Figure SI 7.

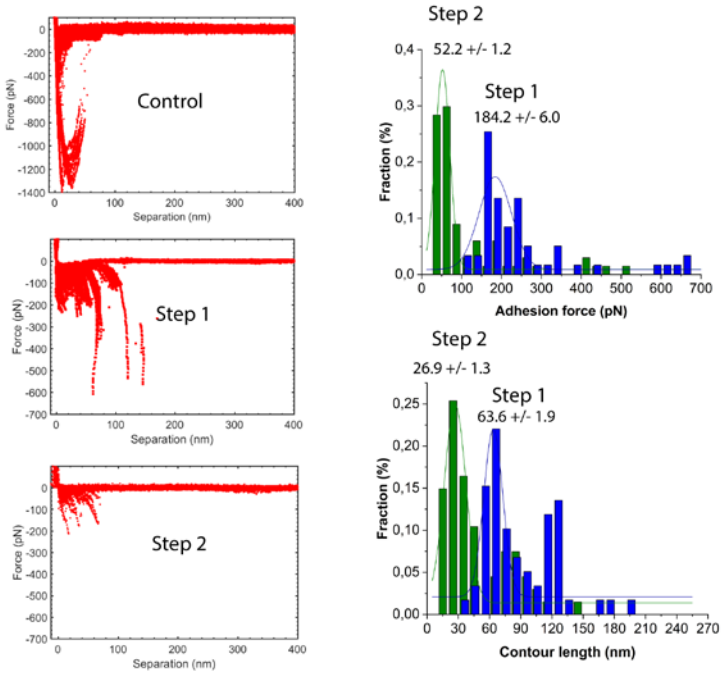

Figure SI 7. Overlap of a series of force distance curves before a) and after tip functionalization with alkyne-PEG-silane (step 1) b) and SpyTag molecule (step 2) c). Histograms with gaussian distribution of adhesion force and contour length are reported for step 1 and 2.

WCA measurements recorded on bare, alkyne and SpyTag functionalized SiO_2 revealed respectively values of ~ 66, 20 and 50 degrees. FT-IR spectra for the PEG-alkyne-silane and SpyTag functionalized SiO_2 showed the characteristic bands of the PEG with slight changes in intensity. The SpyTag coated surface shows an additional weak peak around 1540 cm^{-1}.

The WCA of silane coated SiO_2 surface reveals the amphiphilic nature of the PEG linker. The 3D view of the AFM pictures underline the different height profiles showing that some molecules attached on the surface. Eventually, the FT-ATR IR spectra of the alkyne-PEG-silane coated surface show the charateristic peaks of the PEG chains at 1103, 1735 and 2852 cm^{-1} respectively for C-O-C , C-H and C=O stretching.

When the SpyTag solution is added to the alkyne-PEG-silane coated surfaces, the peaks attributed to the PEG chains are still visible but with lower intensity. The characteristic peak for the triazole absorbtion at 3109 cm^{-1} is not visible, but a weak peak is observed around 1540 cm^{-1} and may be attributed to N=N stretching of the triazole ring (inset of **Figure SI 8d**).

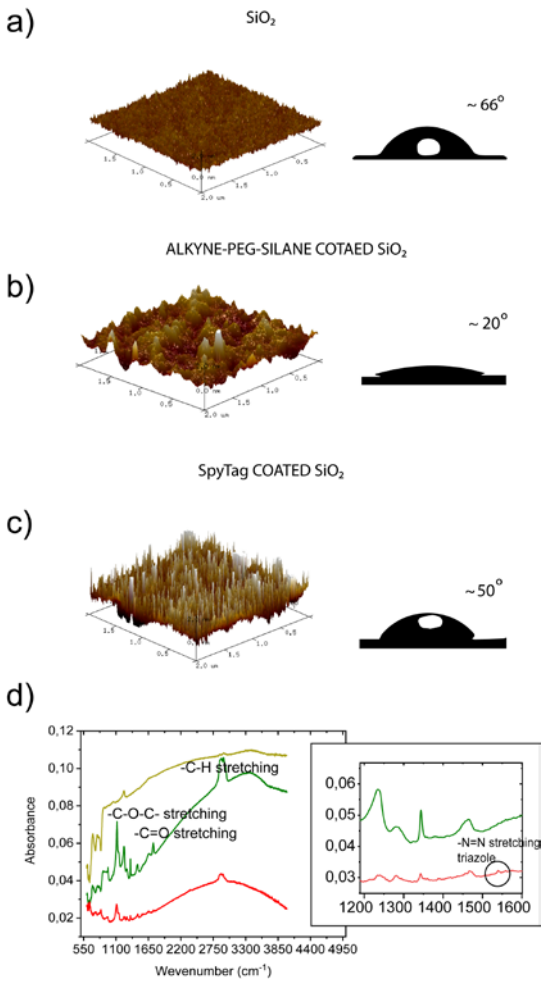

Figure SI 8. AFM images in 3D view and WCA of a) SiO_2 surface, b) alkyne-PEG-silane coated SiO_2, c) SpyTag coated SiO_2 surface previously silanized. d) FT-IR spectra recorded on

SiO_2 surface (dark yellow), silanized surface (green) and SpyTag-functionalized surface (red). The inset represents a zoomed area in the range 1200-1600 cm^{-1}.

Determination of sulfur content in CNC (H_2SO_4)

Sulfate content was determined via conductometric titration . Briefly a solution of protonated CNC, pH 2.88 (133 mg in 500 mL of 1 mM NaCl aqueous solution), are titrated with 100 mM NaOH for 22h (GPD Titrino Metrohm Instrument, tiamo 1.2.1 software).Sulfate half-ester groups content and the sulfur content (%) was calculated using Equation1 and 2, respectively:

$$mmol/kg = V_{NaOH} C_{NaOH}\, m_{CNC} \quad (1)$$

where V_{NaOH} is the inset equivalence point determined from conductometric titration curve, $C_{NaOH}$is the concentration of titrant used and m_{CNC} is the mass of the CNC suspension.

$$\%S = (V_{NaOH} C_{NaO}(S)/\, m_{susp} C_{susp})\; x\; 100 \quad (2)$$

where m*susp* and C*susp* are the mass and concentration (mass %) of the CNC suspension and Mw (S) is the atomic mass of sulfur.

The estimated content of sulfate groups in CNC is 278 mmol*kg^{-1} (0.33 %S).

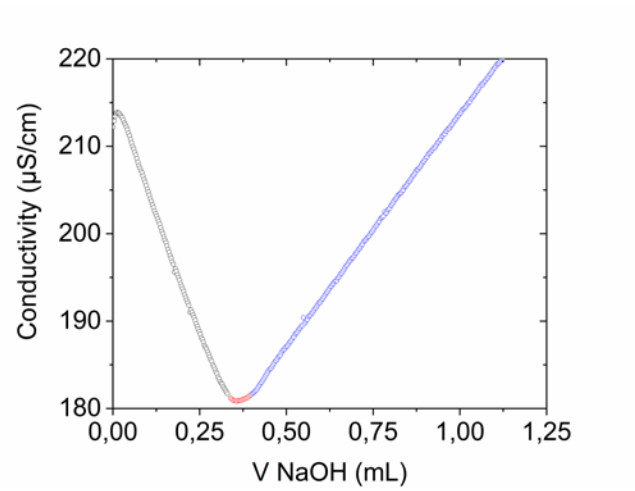

Figure SI 9. Graph reporting conductivity vs volume of the titrant added. Conductivity decreases as the protons associated with the acid sulfate esters are consumed and replaced by sodium cations (grey line), and increases once the volume of added NaOH exceeds the amount required for neutralization (blue line). The red segment represent te neutralization region.

Approach curves of the CNCs

The comparison of the force-distance curves measured at approach revel that there is more repulsion between the tip and the sulfuric acid-hydrolyzed CNCs that with the hydrochloric acid-hydrolyzed CNCs. A sample of 120 approach curves are plotted in Figure SI 10.

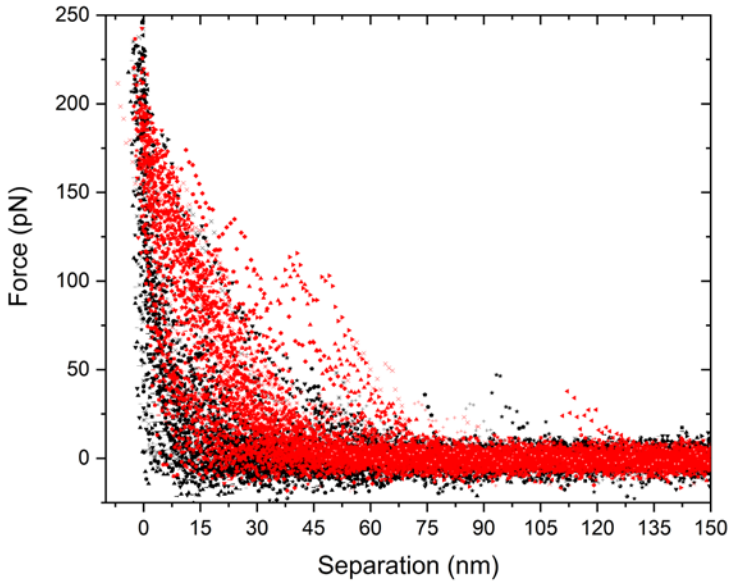

Figure SI 10. Overlap of 120 F_d approaching curves representing the interaction between the SpyCatcher-Cel7A-CBM1 - CNC(HCl) (black dots) and SpyCatcher-Cel7A-CBM1 - CNC(H_2SO_4) (red dots). The larger separation range for the interaction with sulfate-derivatized CNCs is explained by a higher repulsive effect due to the negative charges on the nanocrystals.

References

(1) Lee, C.-D.; Sun, H.-C.; Hu, S.-M.; Chiu, C.-F.; Homhuan, A.; Liang, S.-M.; Leng, C.-H.; Wang, T.-F. An Improved SUMO Fusion Protein System for Effective Production of Native Proteins. *Protein Science 17* (7), 1241–1248.

(2) Engler, C.; Kandzia, R.; Marillonnet, S. A One Pot, One Step, Precision Cloning Method with High Throughput Capability. *PLOS ONE* **2008**, *3* (11), e3647.